Fluorescence Lifetime Control of NV Centers in Nanodiamonds for Long-Term Information Storage

Christian Laube,[*1,2] Robert Temme,[1,2] Andrea Prager,[1] Jan Griebel,[1]

Wolfgang Knolle,[1] and Bernd Abel[1,2]

1) Leibniz-Institute of Surface Engineering (IOM), Permoserstraße 15, 04318 Leipzig, Germany
2) Institute of Chemical Technology, University Leipzig, Linnéstrasse 3, 04103 Leipzig, Germany

*Corresponding author: christian.laube@iom-leipzig.de

Abstract

Today's huge amount of data generation and transfer induced an urgent requirement for long-term data storage. Here, we demonstrate and discuss a novel concept for long-term storage using NV centers inside nanodiamonds. The approach is based upon the radiation-induced generation of additional vacancies (so-called GR1 states), which quench the initial NV centers, resulting in a reduced overall fluorescence lifetime of the NV center. Using the tailored fluorescence lifetime of the NV center to code the information we demonstrate a "beyond binary" data storage density per bit. We also demonstrate that this process is reversible by heating the sample or the spot of information. This proof of principle shows that our technique may be a promising alternative data storage technology, especially in terms of long-term storage due to the high stability of the involved color centers. In addition to the proof of principle demonstration using macroscopic samples, we suggest and discuss the usage of focused electron beams to write information in nanodiamond materials, to read it out with focused low-intensity light, and to erase it on a macro, micro, or nanoscale.

1. Introduction

Diamond and nanodiamond (ND) crystals containing color centers are unique media with a large potential for a wide range of photonics applications due to their thermal and photochemical stability, as well as interesting optical properties.[1],[2] The extreme properties and multifunctionalities also enable numerous applications ranging from the fabrication of long-lasting machining and cutting tools to biomedical coatings, and high-power electronics.[3], [4] Diamond typically contains impurities and other defects whose varying concentration and composition give gems their characteristic colors.[5] Defects of emerging importance are nitrogen vacancy (NV) centers and, in particular, the negatively charged nitrogen vacancy (NV^-) center, a spin 1 complex, formed by a substitutional nitrogen atom adjacent to a vacant site.[6] These paramagnetic defect centers can be initialized through optical pumping, and read out through spin-dependent photoluminescence measurements.[7] Optical access and control of spins and their coherence spin lifetimes have led to recent demonstrations of entanglement and basic quantum logic under ambient conditions, as well as various forms of nanoscale sensing.[8], [9]

Current available digital storage media, which manage and store data are limited in terms of future demands. [10-13] For instance, devices based on binary data storage, such as hard disk drives, flash drives, CDs, DVDs, or Blu-ray discs could no longer meet the storage volume and shelf life requirements of long-term storage in the future.[10] All these storage devices can hold a few terabytes of data compared to the zettabytes and exabytes of information produced every year.[13] HDDs may last several years on average. DVDs and similar storage devices may last for decades but not hundreds of years.[10] Rewritable disks may even fail on each rewrite. With the growing amount of data storage required for our daily lives, and currently available technology being almost saturated, we are in desperate need of a new method of data storage.[14], [15]

Recently, diamond materials were discussed as a promising material to achieve close to eternal data storage lifetimes. Kalbitzer discussed the application of doped diamonds as permanent data storage media with high pixel density based on experimental results, including optical transmission and

luminescence, photo-thermal deflection spectroscopy, infrared and Raman spectroscopy, and ion beam channeling in conjunction with atomic force measurements.[16], [17] Thomas et al. applied ND within a fluorine-doped tin oxide, ND, and silver electrode architecture for resistive random access memory.[18] Ueda et al. demonstrated that graphene/diamond (carbon sp^2/sp^3) heterojunctions can be utilized as multibit optoelectronic memory.[19] Color centers inside the diamond, such as the NV centers, offer interesting properties for data storage application, such as, high stability and optical properties. So far the luminescence of the color center has been applied mostly for labeling applications.[20] In several reports and applications of the past decade, the NV^- center has been investigated and addressed for data storage.[21] Shim et al. presented experimental data on a quantum memory consisting of a single ^{13}C nuclear spin that is strongly coupled to the electron spin of a NV center in a diamond with a fidelity of 88 % for the write-storage-read cycle.[22] More related to long-term data storage, Dhomkar and co-workers studied the optically induced conversion of the NV^- and NV^0 charge states in diamond and realized that NVs can be exploited as nanoscopic classical binary bits with 'ones' and 'zeroes' associated with each charge state.[23]

In the recent past, fluorescence and fluorescence lifetime control have been suggested as a powerful concept for data storage.[13], [24], [25] So far previously investigated inorganic and organic molecular systems and nanomaterials, where the focus was predominantly on inorganic fluorescent materials containing lanthanides and transition metals ions did not yet keep their promise.[26-28] The luminescence lifetime control was achieved with up-conversion, or energy transfer processes depending upon the local environment and structural changes.[27] For example, Algar and Chen et al. investigated the energy transfer between lanthanide complexes and semiconductor quantum dots, leading to a photoluminescence lifetime platform for bioanalysis, imaging, and information storage applications.[29], [30] Concerning the aspect of data storage Lu *et al.* reported a multiplexing concept for information encoding via luminescence decay lifetimes employing 40 nm $NaYF_4$: Yb, Tm nanocrystals with varying amounts of Tm.[31] Liu *et al.* used Mn^{2+} ions and lanthanide-doped nanoparticles as a platform for binary codes.[32] Fluorescence lifetime control for coding and deciphering has been

demonstrated for classes of nanoparticles, such as graphene oxide films,[33] carbon dots,[34] and perovskite nanocrystals.[35]

However, despite these advances new alternatives for data storage and robust long-term data storage are still needed. This is the starting point and motivation of our approach. In the current paper, we first report our concept of enhancing the concentration of NV states in any diamond material by at least one order of magnitude through irradiation and annealing. The lifetime distribution of NV centers can be controlled in turn by a second electron radiation step to form a stable GR1 center without annealing. We use cost-effective diamond nano- or microparticles in the form of a dense pellet for electron beam-controlled lifetime applications, i.e., writing of information into these spots. The nanodiamond surfaces are functionalized by our recent protocols.[36] After a proof-of-principle with multiple writing, reading, and erasing cycles, we aim to discuss possibilities for micro- and nanoscale applications. Finally, we discuss the question of whether fluorescence lifetime controlled nanodiamonds could be a good material for extended time data storage.

2. Results and Discussion

2.1 Nanodiamonds in pellet form, irradiation, functionalization, and its characterization

Nanodiamonds with an oxidized surface, prepared as described elsewhere, were post-treated via variable electron irradiation and annealed at 800 °C in argon atmosphere and subsequent air treatment at 620 °C.[37] Because of the increasing conversion of nitrogen centers (P1 center) and vacancies to NV centers after annealing the fluorescence lifetimes of the NV centers increase with increasing irradiation fluence due to the absence of the main 'quenchers', i.e., the P1 (nitrogen) and the GR1 (vacancy) center (see ESI-SI2).[38], [39] Using this approach nanodiamonds with known surface functionality and a defined fluorescence lifetime distribution of the NV centers can be generated (see ESI-SI2c), displaying a non-linear saturation type trend as a function of the applied fluence. It is well-known that NV centers can appear in two fluorescent charge states, i.e., the NV^- and the NV^0.[40] Both differ in their energetic positions within the lattice, concerning their ground state and their relative

energy to the bandgap of the diamond. As a result, both charge states are differently affected by the presence of P1 centers and other defects, such as the GR1 center.[37] They exhibit slightly different lifetime distributions as a function of the applied e-beam fluence.[40], [37] Nevertheless, the general trend and our argumentation used for the NV^- center can also be applied to the NV^0 charge state. Furthermore, it is also known that the fluorescence decay of NV-states in diamonds is usually biexponential in nature.[41] We assume, in accordance with the literature, that the two lifetimes are due to two possible different quenching effects which we attribute to being located at the surface and inside the nanoparticle lattice.[40] Their dependence on e-beam fluence is rather similar. Therefore, we base our argumentation on the longer fluorescence lifetime component only. As will be highlighted below, this is not a complication, but an advantage because both lifetimes can be controlled and read out, resulting in more information for one diamond spot or a diamond particle.

A comprehensive characterization of the utilized nanodiamonds in terms of particle size, surface functionality, and other features was performed to relate the lifetime changes after irradiation to interactions of the NVs with the new defects inside the nanodiamond (figure 1 and ESI-SI1). In figure 1a the scanning electron micrographs of the nanodiamond-based pellet are displayed at different length scales. The nanodiamonds with sizes below 50 nm are observable at the highest magnification. The infrared spectra of the particles are displayed in Fig. 1b. The spectra indicate that the diamond surface consisting of oxygen-related functionalities such as carboxylic, hydroxylic, and carbonylic groups, remains mostly unchanged after the different irradiation, annealing/heating at air atmosphere protocols applied in our study.[36-37, 42] Furthermore, the absence of surface graphite was approved via X-ray diffraction measurements after each treatment (ESI-SI1).

2.2 Fluorescence lifetime control with post electron irradiation

The GR1 center in diamonds is a common optical defect center created by ionizing radiation exposure and attributed to the neutral monovacancy of the carbon atom (V^0).[43] These centers are luminescent and thermally stable at temperatures of several hundred degrees Celsius. The center has a tetrahedral (T_d) point symmetry. The transition between the lowest ground level ^1E to the first excited state $^1T_2$

features a sharp zero phonon line (ZPL) at 1.673 eV (741 nm) with a phonon-assisted absorption band within the red spectral region. The PL lifetime of the GR1 center was reported to be 1.1 ns at 300 K.[44] Interestingly, there is a lack of investigation targeting the interactions between the GR1 center and NV center as for most applications the GR1 center is seen as an impurity, which can be removed or healed via annealing.[45] Here, we make use of the GR1 center(s) to control/quench the fluorescence of the NV center. After further irradiation of the previously e-beam treated and annealed nanodiamond samples containing a predefined and enlarged number of bright NV centers, we find that many new GR1 centers are created in the lattice environment next to the NV centers (see Fig. 2a). The higher the applied fluence the higher is the concentration of GR1 centers. The luminescence spectra after excitation with 633 nm are displayed in Fig. 2b. A near linear dependence of the GR1 center concentration as a function of e-beam fluence is observed, as indicated by the luminescence intensity ratio at 800 nm (GR1) and 650 nm (NV^- center) (Fig. 2c). The fluorescence lifetime distributions of NV^- centers change accordingly, resulting in a gradual shift of the maximum of the lifetime distribution towards smaller values (see Fig. 2d and e). This effect is attributed to the interaction and quenching of NV^- center luminescence due to defect centers, such as the GR1 centers. GR1 centers are the dominant defect centers under the current experimental conditions and radiation protocols. Although the exact nature of the interaction of NV centers and GR1 centers is not completely clear now, we assume a shorter radiative decay of the NV^- centers due to quenching of NV-center fluorescence due to interactions with nearby GR1 centers in their lattice environment. A dipolar interaction was excluded because a GR1 emission could not be observed upon NV center excitation.[37] This can be rationalized simply from kinetic reasons, i.e., the total depopulation rate of the NV excited state is faster due to GR1 interaction/quenching likely through a non-radiative process, which manifests itself in a shortening of the fluorescence decay. This is the main effect that can be used to control fluorescence lifetimes in diamond materials or nanodiamonds with different radiation doses.

2.3 Defect healing and "resetting" the fluorescence lifetimes

As displayed in Fig. 3a the GR1 centers are generated via e-beam irradiation. In a near linear fashion, we observe more GR1 centers with increasing e-beam fluence. The high stability of the GR1 center is due to the high activation energy of > 1.7 eV, which is required for vacancy diffusion inside the diamond lattice.[46] However, if the diamond material containing GR1 centers is heated to temperatures above 600 °C, the GR1 centers become mobile and diffuse to the surface of the nanoparticles, where they are lost (Fig 3a). This removal of the quenchers would be one interesting possibility to achieve a restoring/reset option towards the original NV fluorescence lifetime. Vacancy defect centers in diamonds can be mobilized at high temperatures above 600 °C. Räcke *et al.* discussed the vacancy diffusion inside diamonds using implantation experiments in combination with random walk simulations.[47] They determined the probability of the loss of the vacancies at the surface at higher temperatures to be at least three orders of magnitude higher than forming an NV^- center with an available nitrogen center (P1). For the optimal set point of the vacancy healing, the stability of the ND particles and a kinetic diffusion simulation of the vacancies model as discussed by Orwa et al. was taken into consideration (ESI-SI5).[46] The stability of the particle at the high temperature regime was monitored using a thermo-gravimetric analysis (ESI-SI4). For the Arrhenius-type diffusion model an activation energy of the vacancy diffusion of about 1.7 eV was used. Under room temperature conditions due to this high activation energy of the vacancy no diffusion, and thus, information loss can be expected. An optimal set point for vacancy healing was determined to be 620 °C. At this temperature, the material loss was less than 0.6 %. The simple Arrhenius model suggested that a complete GR1 center removal may be expected within one hour (ESI-SI5). If the diffusion towards the surface is the main decay channel for the vacancy defects, a neglectable impact on the optical properties of NV^- centers after the heating can be expected. Such a reversible cycle is displayed in Fig. 3b. While irradiation shifts the lifetimes towards smaller values the high temperature led to higher lifetime distribution due to GR1 center healing. For the experiments, we started from a "Standard" ND pellet (irradiated with a fluence of $2 \cdot 10^{18}\,cm^{-2}$ at 800 °C, and subsequent air oxidization at 620 °C). For

the desired lifetime control the sample was irradiated with a predefined fluence of > $1 \cdot 10^{18}$ cm^{-2}. Due to an achievable e-beam irradiation dose of $1 \cdot 10^{18}$ cm^{-2} per day we limited the series to 3 cycles here. The reset of the luminescence lifetimes was achieved via heating under air atmosphere at around 620 °C (see Fig. 3b). Under the chosen oxidative condition, no graphitization of the ND surface appears. Furthermore, the surface remains its oxygen-functionalized surface. Nevertheless, after each cycle a small shift towards smaller lifetimes can be observed. This effect might be related to the different defect structures, such as divacancies or vacancy clusters, and will be discussed in section 2.5.[45]

2.4 Macroscopic storage of information through precise fluorescence lifetime control and optical readout

A first proof of principle for reversible information storage employing nanodiamond NV center luminescence lifetimes is illustrated in Fig. 4. The range of luminescence lifetime values detectable in our experiment may be converted into the characters of the extended American Standard Code for Information Interchange format (ASCII) by using standard character table.[48] The approach can be understood as follows: the NV center fluorescence lifetimes, resolvable with our setup, may be sorted into four different lifetime windows. Each lifetime regime is converted into what we call "lifetime conversion value (LCV)" between 0 and 3: LCV (0): (< 12 ns), LCV (1): (12-15 ns), LCV (2): (15-18 ns), LCV (3): (>18 ns). This establishes a four digit coding system corresponding to the four LCVs.[49] The extended ASCII character table includes 256 characters that can be ciphered by the four time bits in a quaternary coding system, $256 = 4^4$. To apply the ASCII table, the quaternary code first needs to be linked to a number between 0 - 255 using:

$$\mathrm{N}(\textit{Decimal}) = \mathrm{w} \cdot 4^0 + x \cdot 4^1 + y \cdot 4^2 + z \cdot 4^3 \qquad (1)$$

Herein, w, x, y, z denotes the LCVs between 0–3. The determined number between 0–255 can then be assigned to a character according to the ASCII standard extended character table in analogy to the binary or decimal numeral system (see Figure 4a and b). The experimental realization of the data ciphering was established in a macroscopic approach using ND pellets with precisely controlled NV luminescence lifetime distributions with a defined maximum (Figure 4c). The overall full width at half

maximum of the lifetime time distribution was determined to be (5.5 ± 1) ns. This value is a limiting factor of the lifetime decoding approach and was the reason why only a quaternary code was applied for the data ciphering. In an ideal situation, an information bit should be correlated with an as-small-as-possible lifetime distribution and an as- fast-as possible decay time, while exhibiting a high quantum yield to enable high performances of data storage with a high information density, and a short read-out time. Figures 4d–e illustrate the fluorescence lifetime distributions of pellets that encode the word "Hello". The corresponding fluences of the "writing step" irradiation were ϕ (LCV (0)): $2 \cdot 10^{18}$ cm^{-2}, ϕ (LCV (1)): $1 \cdot 10^{18}$ cm^{-2}, ϕ (LCV (2)): $0.25 \cdot 10^{18}$ cm^{-2} and ϕ (LCV (3)): $0 \cdot 10^{18}$ cm^{-2}. For each character four ND pellets with their LCVs were arranged in a cyclic fashion here, for simplicity. The readout starts per definition from the right side and proceeds clockwise, as displayed in Fig. 4d, e. The shown data demonstrate the successful application of luminescence lifetime control inside macroscopic ND patterns to store information beyond the traditional binary level.

The demonstrated examples depend crucially on the radiation protocol including the radiation dose, the annealing parameter, surface functionalization, and particle size. In Figure (ESI-SI3) a similar effect is displayed for a particle size of 250 µm, where the variation of lifetime distribution between the sample with and without second irradiation is narrower. The radiation induced quenching effect can be even nicely seen in the time resolved fluorescence traces (Figure ESI-SI3 (d)). In any case, we have shown that writing, encoding, reading, and erasing data on nanodiamond material is a new highly complex process, but one which is robust and with a simple foundation. Furthermore, it can be extended beyond a binary system to store information.[23]

2.5 From macro- to micro- and nanoscale information storage

In the previous parts, we could demonstrate the realization of storage of information via e-beam irradiation, optical readout of information with light, and erasing of information via heat on a macroscopic nanodiamond particle sample in pellet form. We have also shown that the same concept also works with 250 µm particles (ESI-SI3). In the following, we would like to discuss critically the potential of the concept and – in particular – if such a concept can be translated and applied also to

the micro- or nanoscale. It should be emphasized here that since our process is in an early phase of development, only the purely scientific feasibility and no commercial aspects are taken into account in the discussion.

Regarding the requirements on the properties of NV centers containing NDs for long-term data storage two general challenges were revealed during the macroscopic experiment. First, the width of the lifetime distributions, second, the slightly incomplete lifetime recovery during the annealing process. The broadening of the lifetime distributions is caused by several parameters, among others the diversity of the particle shape, and the statistical distribution of the NV centers in the particles. In general, these parameters affect the application of NDs in various fields. A higher homogeneity of the NDs in terms of their shape and color center distribution should have a significant impact on the fluorescence lifetime distribution of the NV centers. This statement is further strengthened by the investigations of the 250 µm diamond samples. For this particle size, the surface is expected to have a low impact on the fluorescence lifetime due to the surface-to-volume ratio and we determined the FWHM of the fluorescence distribution to be just 2.5 ns. Therefore, current new synthesis methods for ND target a higher homogeneity in terms of their size and shape and color center concentration.[50] With regard to the distribution statistics of the number of color centers in the ND particles, the current results on the deterministic implantation of color centers in diamonds promise to solve this challenge for bulk diamonds. Alternatively to the application of ND, micro and nanoscale diamond columns could also be used, in which color centers could be implanted with high precision.[51]

We assume the reason for the incomplete recovery of the fluorescence lifetime during the defect healing process to be the formation of divacancies and vacancy clusters.[45] To the best of our knowledge, a direct effect of these centers on the fluorescence lifetime of the NV center was not discussed in the literature so far. These centers are discussed to be more stable than single vacancy and exhibit a negative effect on the coherence time of NV centers. To avoid the formation of these defects, irradiation is currently being tested under a wide variety of conditions. Lühmann et al. discussed the hindering of the formation of divacancy via doping of the bulk diamonds.[52] At this point

we want to mention, that a direct relation of the incomplete fluorescence lifetime recovery to the formation of divacancies and vacancy clusters is beyond the scope of this manuscript. Nonetheless, the effect must be considered as a possible limiting factor, especially in cases where several resetting cycles should be performed. It should be noted that the use of multiple resetting cycles is rather atypical in long-term data storage. Studies on how to avoid these centers will be the subject of subsequent work.

In the following, we briefly discuss the realization of a miniaturized data storage concept. The three requirements for data storage, i.e., data writing, data readout, and data deletion, require electrons, photons irradiation, and local heating as outlined above. On the nanoscale, high doses of electrons required for data writing can be applied with a focused electron beam (FEB). A focused electron beam as applied within electron lithography or within a TEM should be suitable for the manipulation of nanodiamonds on a nanoscale as demonstrated for bulk diamonds by Steeds et al. (see Fig. 5b).[53] Kalbitzer emphasized that by applying focused ion beams on diamonds effective pixel writing of dimensions as small as 10 nm (about 1 and 100 Tbit, respectively, on a 100 cm^2 disc) is possible. [16] The doses have to be scaled according to the irradiation protocols established here, in a way to avoid burning of the nanodiamonds in the FEB. Electron densities in a TEM can be as high as 600 $e/(Å^2 \cdot s)$ corresponding to $6 \cdot 10^{22}$ $e^-/(cm^2 \cdot s)$.[54] This is quite high compared to the required dose necessary for the GR1 center formation, such that this could theoretically be realized within the ms to µs regime. At the same time, the particles could easily be degraded or surface modified, thus a compromise between destruction and information encoding has to be found. Also, Schwartz et al. pointed out that the defect generation at lower kinetic electron energies in FEBs might differ from the MeV regime.[55]

The photons for the readout of the fluorescence lifetime can be applied easily within the focus of a suitable light source (see figure 5b), being within the diffraction limit.[37] For the readout of information in single particles a focused laser can be employed to excite the luminescence. Photons can then be recorded via single photon counting technology.[56] Such an approach (focusing electrons and photons) is limited by space charge repulsion and the diffraction limit for the readout. Although, electron beam

focus and super resolution technologies such as STED or STORM can overcome the diffraction limit in the write and readout steps, in normal applications larger areas are addressed, which may still be sufficient for a technology push in terms of storage density and ultra-long term durability.[57], [58] Another technique that enables high lateral resolution, and thus, is suitable to read out the lifetime information down to the nanoscale is the single pulse cathodoluminescence.[59] Nevertheless, for all subdiffractional limit techniques the relatively low scanning rate needs to be mentioned as a still present challenge. Another conceptual challenge is the miniaturization of the erasing step, which requires a localized high energy input. The simple complete macroscopic erase of all stored data could be realized via a thermal treatment as performed in this work. For local and microscopic heating of, for example a ND Array, a focused continuous wave or pulsed laser light can be applied, such as demonstrated, previously.[1] By varying the duration and intensity of the laser pulse in a single spot we can control the heat in a defined fashion. Nonetheless, the heat diffusion within the ND array needs to be probed carefully. Therefore, several ways to monitor the local temperature of NDs via the Raman signal or the fluorescence intensity were already discussed in the literature and could be applied for the evaluation of the heat diffusion.[1], [60]

3. Conclusion and Outlook

The idea behind our approach highlighted here is that cheap nanodiamonds of nearly any size in the form of pellets may be irradiated by an e-beam with subsequent annealing such that the luminescence lifetimes of NV centers are altered in a defined way, which may in turn be employed for durable information storage in the material. The information may be read out by light and erased by heat. Although our example above is currently macroscopic in nature, still limited conceptually, and may not perform yet up to the highest levels, the results shown here are indeed very promising as a proof-of-concept. As discussed, the high stability of the involved color centers estimated via a simple Arrhenius diffusion model appears to be interesting for optical long-term data storage in diamonds. Theoretically, the estimates on defect stability suggest storage-duration even beyond centuries, which would be an alternative to traditional devices. Concerning a hypothetical data storage capacity, the demonstrated

approach may exceed and outperform binary data storage approaches in the future. The practical implementation, however, still needs to be investigated and established to enable the miniaturization and writing-erasing-cycle stability of the system. The miniaturization, and thus, improvement and evaluation of the data-storage capacity of the system will be the subject of future research.

4. Experimental Section

4.1 Nanodiamond material and irradiation protocols

The starting material for measurements was aqua regia cleaned MSY 0.0 – 0.05 NDs (Microdiamant AG, Switzerland) (GND) with a nitrogen content of around 100 ppm. The GND were cleaned in an initial step using air etching at 590 °C (1 atm) for 17 hours to produce graphite-free oxidized NDs (OND) with a diameter below 30 nm as measured by Scanning Electron Microscopy (SEM). 5 mg of OND-sample were pressed using a 3 mm diameter press cell container, for irradiation. After irradiation with at least $2–3 \cdot 10^{18}$ cm^{-2}, the samples were post-treated by annealing in an argon stream (50 ml/min) for 5 hours at 800 °C followed by a second air etching step at 620 °C to produce ND with a saturated fluorescence lifetime according to Ref.[37] For the lifetime control, an additional irradiation step without post-treatment was performed.

4.2 Electron Beam Irradiation of NDs

The NDs were irradiated with 10 MeV electrons from a linear electron accelerator (MB10-30MP - Mevex Corp., Stittsville, Canada), as pellets in an aluminum vessel. The irradiation was performed with a dose rate of 20 kGy/min. An air-cooling system was employed to prevent sample temperatures above 250 °C during irradiations. The dose rate was determined with a radio chromic foil dosimeter (B3-film, GEX-Corp.) and the number of electrons per cm^2 (fluence) was calculated from the applied total dose assuming an average stopping power of 2 MeV $\cdot$ $cm^2 \cdot g^{-1}$ at the nominal electron energy of 10 MeV.

4.3 Scanning Electron Microscopy (SEM)

Scanning electron microscopy (SEM) images were taken using an ULTRA 55 (Carl Zeiss SMT) scanning electron microscope. An accelerating voltage of 2 kV was applied. All samples were investigated without an additional conductive layer.

4.4 Attenuated Total Reflection Infrared Spectroscopy (ATR-IR)

The infrared spectra were measured using a VECTOR 22 (Bruker) combined with an attenuated total reflectance module ("Golden Gate", Graseby, Specac). For all samples, 128 scans were averaged. For measurements, the nanodiamond powder was deposited onto the diamond window without any pre-treatments.

4.5 Thermogravimetric analysis (TGA)

For the TGA measurement, a Pyris 1 (PerkinElmer) Thermo-gravimeter was used, and the heating rate was 10 K/min under air atmosphere for the temperature range from 50 °C to 900 °C.

4.6 Fluorescence spectra and fluorescence lifetime imaging

The fluorescence spectra of the NV centers were recorded using a Horiba LabRam HR Evolution spectrometer equipped with an Olympus MPlan 10x/ NA = 0.25 objective, a 600 $l \cdot mm^{-1}$ grid, and a Synapse detector. A second harmonic Nd:YAG laser (wavelength of 532 nm) and diode laser of 633 nm were applied as excitation light.

The applied confocal setup for the fluorescence lifetime imaging microscopy (FLIM) consists of a DCS-120 FLIM system (Becker and Hickl) in combination with an Olympus XI 71 microscope. A pulsed diode laser (513 nm wavelength, 60 ps pulse duration, 20 MHz repetition rate, Becker & Hickl) was employed. The light was focused and collected in backscattering geometry by a 10× objective (Olympus LUCPlan FLN 10x, NA 0.3). The FLIM measurement of the pellet areas was observed for a lateral window of 1.8 mm x 1.8 mm. For the selective detection of the NV^- fluorescence, a combination of a 647 nm long pass and a 710 nm bandpass filter was used. To determine the fluorescence lifetime at each data point,

the time profiles were fitted via a bi-exponential fitting approach provided by the SPC-image software (Becker & Hickl). In the case of longer fluorescence lifetimes, the fluorescence lifetime was recalculated using the incomplete decay method implemented in the SPC-image software that includes a correction for the high repetition rate for the laser excitation. These fluorescence lifetimes were used to create a location (pixel) related decay matrix (fluorescence lifetime image) and a corresponding fluorescence lifetime histogram. The resulting mean fluorescence lifetimes were utilized for the fluorescence lifetime to fluence comparison.

Supporting Information

Supporting Information is available through the authors and the journal web page.

Acknowledgments

The Authors thank the German Science Foundation (DFG) for support through SFB-TR102 and FOR 2177 and the BMBF/ZIM program through the grant "SafeLabel, No KK5030502EB0".

Conflict of Interest

The authors declare no conflict of interest.

Data Availability Statement

Research data are available upon reasonable request from the authors.

Keywords

Nitrogen vacancy center, luminescence lifetime distribution, irradiation, nanodiamonds, read-write-erase, long-term data storage

References

[1] C. Laube, J. Hellweg, C. Sturm, J. Griebel, M. Grundmann, A. Kahnt, B. Abel, *The Journal of Physical Chemistry C* **2018**, *122*, 25685-25691.

[2] N. Bondon, L. Raehm, C. Charnay, R. Boukherroub, J.-O. Durand, *Journal of Materials Chemistry B* **2020**, *8*, 10878-10896.

[3] M. Radtke, E. Bernardi, A. Slablab, R. Nelz, E. Neu, *Nano Futures* **2019**, *3*, 042004.

[4] V. N. Mochalin, O. Shenderova, D. Ho, Y. Gogotsi, *Nature Nanotechnology* **2012**, *7*, 11-23.

[5] F. Jelezko, J. Wrachtrup, *Physica status solidi (a)* **2006**, *203*, 3207-3225.

[6] R. Schirhagl, K. Chang, M. Loretz, C. L. Degen, *Annual Review of Physical Chemistry* **2014**, *65*, 83-105.

[7] M. W. Doherty, N. B. Manson, P. Delaney, F. Jelezko, J. Wrachtrup, L. C. L. Hollenberg, *Physics Reports* **2013**, *528*, 1-45.

[8] Y. Wu, Y. Wang, X. Qin, X. Rong, J. Du, *npj Quantum Information* **2019**, *5*, 9.

[9] J. J. Hamlin, B. B. Zhou, *Science* **2019**, *366*, 1312.

[10] A. Nordrum, *IEEE Spectrum* **2020**, *57*, 10-11.

[11] B. Tudu, A. Tiwari, *Vacuum* **2017**, *146*, 329-341.

[12] M. Gu, Q. Zhang, S. Lamon, *Nature Reviews Materials* **2016**, *1*, 16070.

[13] J. Yu, M. Luo, Z. Lv, S. Huang, H.-H. Hsu, C.-C. Kuo, S.-T. Han, Y. Zhou, *Nanoscale* **2020**, *12*, 23391-23423.

[14] S. Jeffrey, *World Archaeology* **2012**, *44*, 553-570.

[15] W. A. Bhat, *Library Hi Tech* **2018**, *36*, 539-555.

[16] S. Kalbitzer, *Applied Physics A* **2001**, *72*, 639-670.

[17] S. Kalbitzer, *Nuclear Instruments and Methods in Physics Research Section B: Beam Interactions with Materials and Atoms* **2004**, *218*, 343-354.

[18] A. Thomas, M. S. Parvathy, K. B. Jinesh, *Carbon Trends* **2021**, *3*, 100023.

[19] K. Ueda, Y. Mizuno, H. Asano, *Applied Physics Letters* **2020**, *117*, 092103.

[20] Y.-T. Chuang, S.-D. Chen, W.-C. Huang, T.-L. Shen, M.-S. Chang, Y.-F. Chen, Y.-P. Hsieh, Y.-H. Chang, M. Hofmann, *ACS Applied Materials & Interfaces* **2020**, *12*, 49006-49011.

[21] B. Grotz, M. V. Hauf, M. Dankerl, B. Naydenov, S. Pezzagna, J. Meijer, F. Jelezko, J. Wrachtrup, M. Stutzmann, F. Reinhard, J. A. Garrido, *Nature Communications* **2012**, *3*, 729.

[22] J. H. Shim, I. Niemeyer, J. Zhang, D. Suter, *Physical Review A* **2013**, *87*, 012301.

[23] S. Dhomkar, J. Henshaw, H. Jayakumar, C. A. Meriles, *Science Advances* **2016**, *2*, e1600911.

[24] Y. Xie, M. C. Arno, J. T. Husband, M. Torrent-Sucarrat, R. K. O'Reilly, *Nature Communications* **2020**, *11*, 2460.

[25] B. Hu, C. Wang, J. Wang, J. Gao, K. Wang, J. Wu, G. Zhang, W. Cheng, B. Venkateswarlu, M. Wang, P. S. Lee, Q. Zhang, *Chemical Science* **2014**, *5*, 3404-3408.

[26] Y. Ma, Y. Dong, P. She, S. Liu, M. Xie, Y. Yu, Y. Li, Q. Zhao, W. Huang, *Advanced Optical Materials* **2018**, *6*, 1801065.

[27] P. She, Y. Ma, Y. Qin, M. Xie, F. Li, S. Liu, W. Huang, Q. Zhao, *Matter* **2019**, *1*, 1644-1655.

[28] H. Huang, J. Chen, Y. Liu, J. Lin, S. Wang, F. Huang, D. Chen, *Small* **2020**, *16*, 2000708.

[29] W. R. Algar, N. Hildebrandt, S. S. Vogel, I. L. Medintz, *Nature Methods* **2019**, *16*, 815-829.

[30] C. Chen, L. Ao, Y.-T. Wu, V. Cifliku, M. Cardoso Dos Santos, E. Bourrier, M. Delbianco, D. Parker, J. M. Zwier, L. Huang, N. Hildebrandt, *Angewandte Chemie International Edition* **2018**, *57*, 13686-13690.

[31] Y. Lu, J. Zhao, R. Zhang, Y. Liu, D. Liu, E. M. Goldys, X. Yang, P. Xi, A. Sunna, J. Lu, Y. Shi, R. C. Leif, Y. Huo, J. Shen, J. A. Piper, J. P. Robinson, D. Jin, *Nature Photonics* **2014**, *8*, 32-36.

[32] X. Liu, Y. Wang, X. Li, Z. Yi, R. Deng, L. Liang, X. Xie, D. T. B. Loong, S. Song, D. Fan, A. H. All, H. Zhang, L. Huang, X. Liu, *Nature Communications* **2017**, *8*, 899.

[33] Z. Qiao, C. Qin, W. He, Y. Gong, B. Li, G. Zhang, R. Chen, Y. Gao, L. Xiao, S. Jia, *Carbon* **2019**, *142*, 224-229.

[34] S. Kalytchuk, Y. Wang, K. Poláková, R. Zbořil, *ACS Applied Materials & Interfaces* **2018**, *10*, 29902-29908.

[35] X.-F. Liu, L. Zou, C. Yang, W. Zhao, X.-Y. Li, B. Sun, C.-X. Hu, Y. Yu, Q. Wang, Q. Zhao, H.-L. Zhang, *ACS Applied Materials & Interfaces* **2020**, *12*, 43073-43082.

[36] C. Laube, Y. M. Riyad, A. Lotnyk, F. P. Lohmann, C. Kranert, R. Hermann, W. Knolle, T. Oeckinghaus, R. Reuter, A. Denisenko, A. Kahnt, B. Abel, *Materials Chemistry Frontiers* **2017**, *1*, 2527-2540.

[37] C. Laube, T. Oeckinghaus, J. Lehnert, J. Griebel, W. Knolle, A. Denisenko, A. Kahnt, J. Meijer, J. Wrachtrup, B. Abel, *Nanoscale* **2019**, *11*, 1770-1783.

[38] D. Gatto Monticone, F. Quercioli, R. Mercatelli, S. Soria, S. Borini, T. Poli, M. Vannoni, E. Vittone, P. Olivero, *Physical Review B* **2013**, *88*, 155201.

[39] G. Liaugaudas, G. Davies, K. Suhling, R. U. A. Khan, D. J. F. Evans, *Journal of Physics: Condensed Matter* **2012**, *24*, 435503.

[40] J. Storteboom, P. Dolan, S. Castelletto, X. Li, M. Gu, *Optics Express* **2015**, *23*, 11327-11333.

[41] B. R. Smith, D. Gruber, T. Plakhotnik, *Diamond and Related Materials* **2010**, *19*, 314-318.

[42] A. Krueger, D. Lang, *Advanced Functional Materials* **2012**, *22*, 890-906.

[43] S. Subedi, V. Fedorov, S. Mirov, M. Markham, *Opt. Mater. Express* **2021**, *11*, 757-765.

[44] A. T. Collins, J. Szechi, S. Tavender, *Journal of Physics C: Solid State Physics* **1988**, *21*, L161-L164.

[45] Y. Mindarava, R. Blinder, C. Laube, W. Knolle, B. Abel, C. Jentgens, J. Isoya, J. Scheuer, J. Lang, I. Schwartz, B. Naydenov, F. Jelezko, *Carbon* **2020**, *170*, 182-190.

[46] J. O. Orwa, K. Ganesan, J. Newnham, C. Santori, P. Barclay, K. M. C. Fu, R. G. Beausoleil, I. Aharonovich, B. A. Fairchild, P. Olivero, A. D. Greentree, S. Prawer, *Diamond and Related Materials* **2012**, *24*, 6-10.

[47] P. Räcke, L. Pietzonka, J. Meijer, D. Spemann, R. Wunderlich, *Applied Physics Letters* **2021**, *118*, 204003.

[48] V. G. Cerf, *RFC0020: ASCII format for network interchange*, RFC Editor, **1969**.

[49] P. Wei, B. Li, A. de Leon, E. Pentzer, *Journal of Materials Chemistry C* **2017**, *5*, 5780-5786.

[50] C.-H. Nee, S.-L. Yap, T.-Y. Tou, H.-C. Chang, S.-S. Yap, *Scientific Reports* **2016**, *6*, 33966.

[51] E. Neu, P. Appel, M. Ganzhorn, J. Miguel-Sánchez, M. Lesik, V. Mille, V. Jacques, A. Tallaire, J. Achard, P. Maletinsky, *Applied Physics Letters* **2014**, *104*, 153108.

[52] T. Lühmann, J. Meijer, S. Pezzagna, *Physica status solidi (a)* **2021**, *218*, 2000614.

[53] J. Steeds, W. Kaiyue, L. Zhihong, *Diamond and Related Materials* **2012**, *23*, 154-156.

[54] M. Ilett, M. S'ari, H. Freeman, Z. Aslam, N. Koniuch, M. Afzali, J. Cattle, R. Hooley, T. Roncal-Herrero, S. M. Collins, N. Hondow, A. Brown, R. Brydson, *Philosophical Transactions of the Royal Society A: Mathematical, Physical and Engineering Sciences* **2020**, *378*, 20190601.

[55] J. Schwartz, S. Aloni, D. F. Ogletree, T. Schenkel, *New Journal of Physics* **2012**, *14*, 043024.

[56] M. D. Lesoine, S. Bose, J. W. Petrich, E. A. Smith, *J Phys Chem B* **2012**, *116*, 7821-7826.

[57] N. Prabhakar, M. Peurla, S. Koho, T. Deguchi, T. Näreoja, H.-C. Chang, J. M. Rosenholm, P. E. Hänninen, *Small* **2018**, *14*, 1701807.

[58] M. Gu, Y. Cao, S. Castelletto, B. Kouskousis, X. Li, *Optics Express* **2013**, *21*, 17639-17646.

[59] J. Ferrer Orri, E. M. Tennyson, G. Kusch, G. Divitini, S. Macpherson, R. A. Oliver, C. Ducati, S. D. Stranks, *Nano Express* **2021**, *2*, 024002.

[60] S. Choe, J. Yoon, M. Lee, J. Oh, D. Lee, H. Kang, C.-H. Lee, D. Lee, *Current Applied Physics* **2018**, *18*, 1066-1070.

Figures & Figure Captions

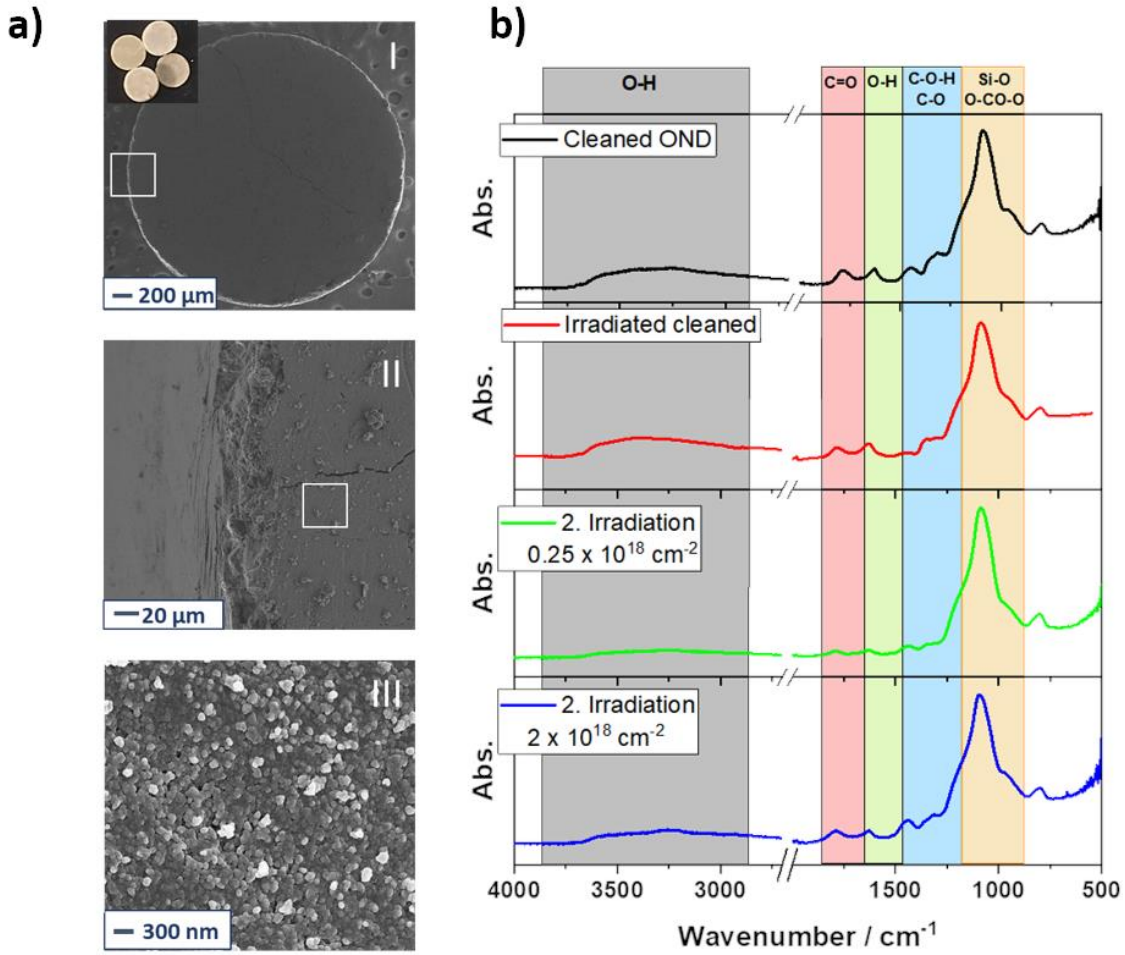

Figure 1 Surface monitoring during the different treatment steps towards the tailoring of fluorescence properties of NV center inside nanodiamonds: **a)** Image of the applied pellets (d = 2mm, inset) as well as SEM images I – III with different scalebar; **b)** ATR-IR spectra of different treated NDs: Black: oxidized graphite free nanodiamond (600 °C, Air), Red: irradiated ($2 \cdot 10^{18}$ cm^{-2}) annealed (800 °C, Ar) and oxidized (620 °C, Air) nanodiamond, Green: irradiated ($2 \cdot 10^{18}$ cm^{-2}), annealed (800 °C, Ar), oxidized (620 °C, Air) nanodiamond and irradiated for a second time ($0.25 \cdot 10^{18}$ cm^{-2}), Blue: irradiated ($2 \cdot 10^{18}$ cm^{-2}), annealed (800 °C, Ar), oxidized (620 °C, Air) nanodiamond and irradiated for a second time ($2 \cdot 10^{18}$ cm^{-2}).

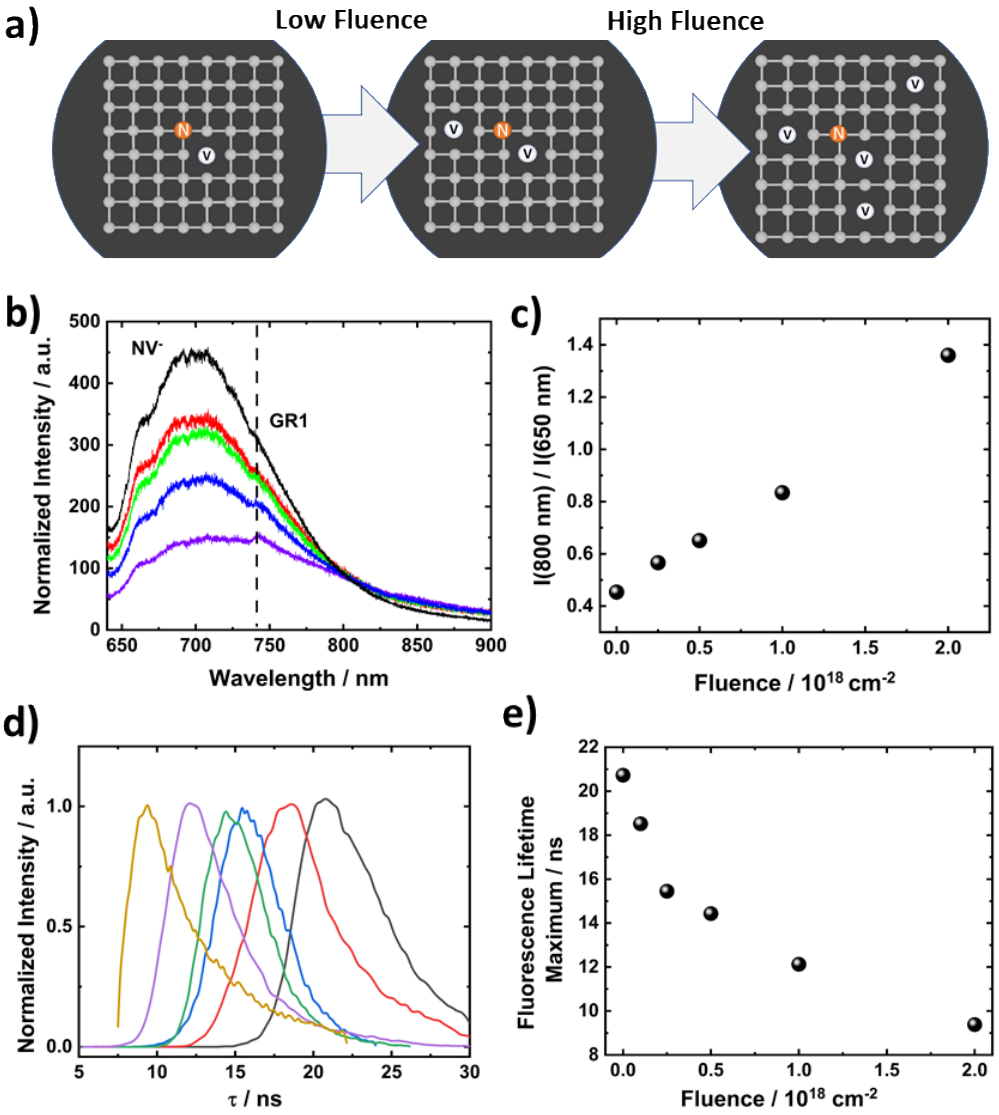

Figure 2 Defect induced NV center lifetime tailoring inside nanodiamonds: **a)** Schematic illustration of the fluence dependent defect generation; **b)** Fluorescence spectra normalized at 800 nm (λ_{ex} = 633 nm) of irradiated ($2 \cdot 10^{18}$ cm^{-2}), Post-treated (800 °C, Ar and 620 °C, Air), and irradiated a second time: Black $\phi = 0$, Red $\phi = 0.25 \cdot 10^{18}$ cm^{-2}, Green $\phi = 0.5 \cdot 10^{18}$ cm^{-2}, Blue $\phi = 1 \cdot 10^{18}$ cm^{-2}, Violet $\phi = 2 \cdot 10^{18}$ cm^{-2}; **c)** Fluorescence intensity ratio of the NV$^-$ center (650 nm) to the GR1 center (800 nm) related fluorescence, note, the 800 nm were selected to ensure a minimum of spectral overlap of the GR1 and the NV center ; **d)** Lifetime distribution histograms (normalized) of ND samples, which were irradiated ($2 \cdot 10^{18}$ cm^{-2}), Post-treated (800 °C, Ar and 620 °C, Air), and irradiated a second time: Black $\phi = 0$, Red $\phi = 0.1 \cdot 10^{18}$ cm^{-2}, Blue $\phi = 0.25 \cdot 10^{18}$ cm^{-2}, Green $\phi = 0.5 \cdot 10^{18}$ cm^{-2}, Violet $\phi = 1 \cdot 10^{18}$ cm^{-2}, Yellow $\phi = 2 \cdot 10^{18}$ cm^{-2}, **e)** Maximum lifetimes to applied fluences during the defect generation step (after second irradiation).

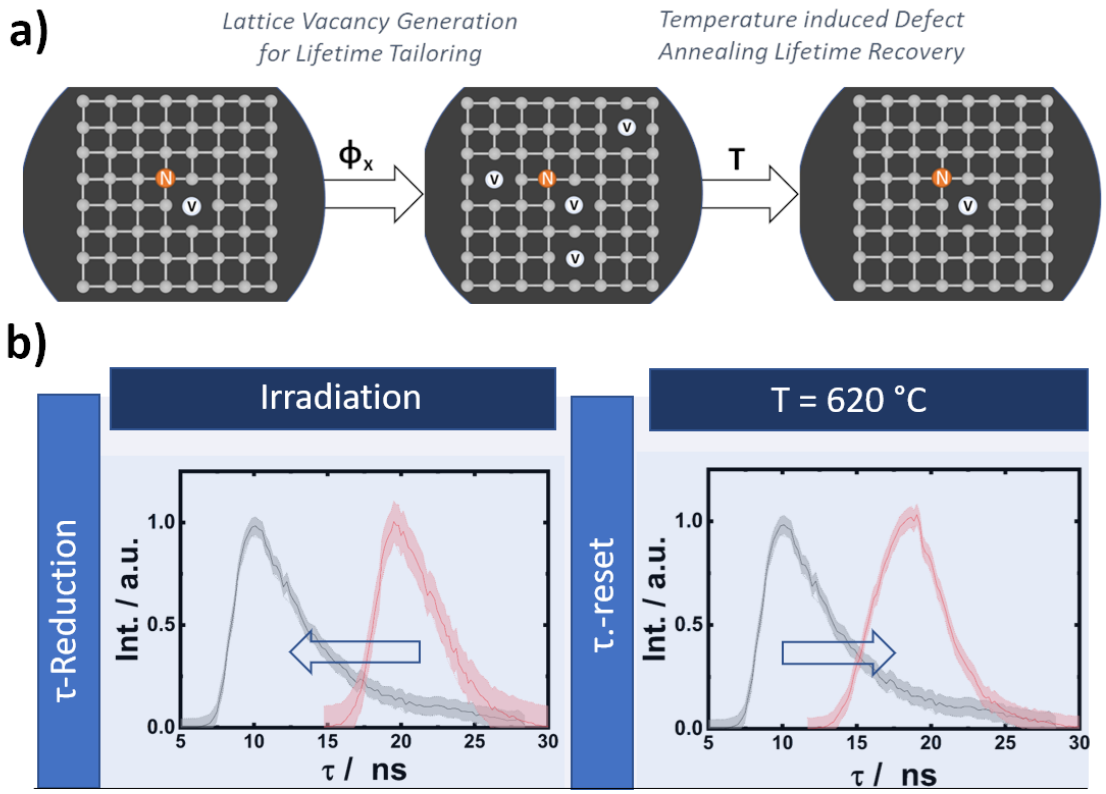

Figure 3 Lifetime code resetting by thermal treatment: **a)** Schematic illustration of the suggested mechanism, defects generated by the irradiation quench the fluorescence of the NV center, the defects can be removed via a high-temperature treatment, and thus, the initial lifetime τ_0 can be regained, **b)** Lifetime histograms illustrating the reversible lifetime adjustment via irradiation ($\phi = 1 \cdot 10^{18}$ cm^{-2}) and high temperature treatment at 620 °C under air atmosphere, the starting material was a ND sample irradiated with $\phi = 2 \cdot 10^{18}$ cm^{-2} followed by argon annealing at 800 °C and air treatment at 620 °C.

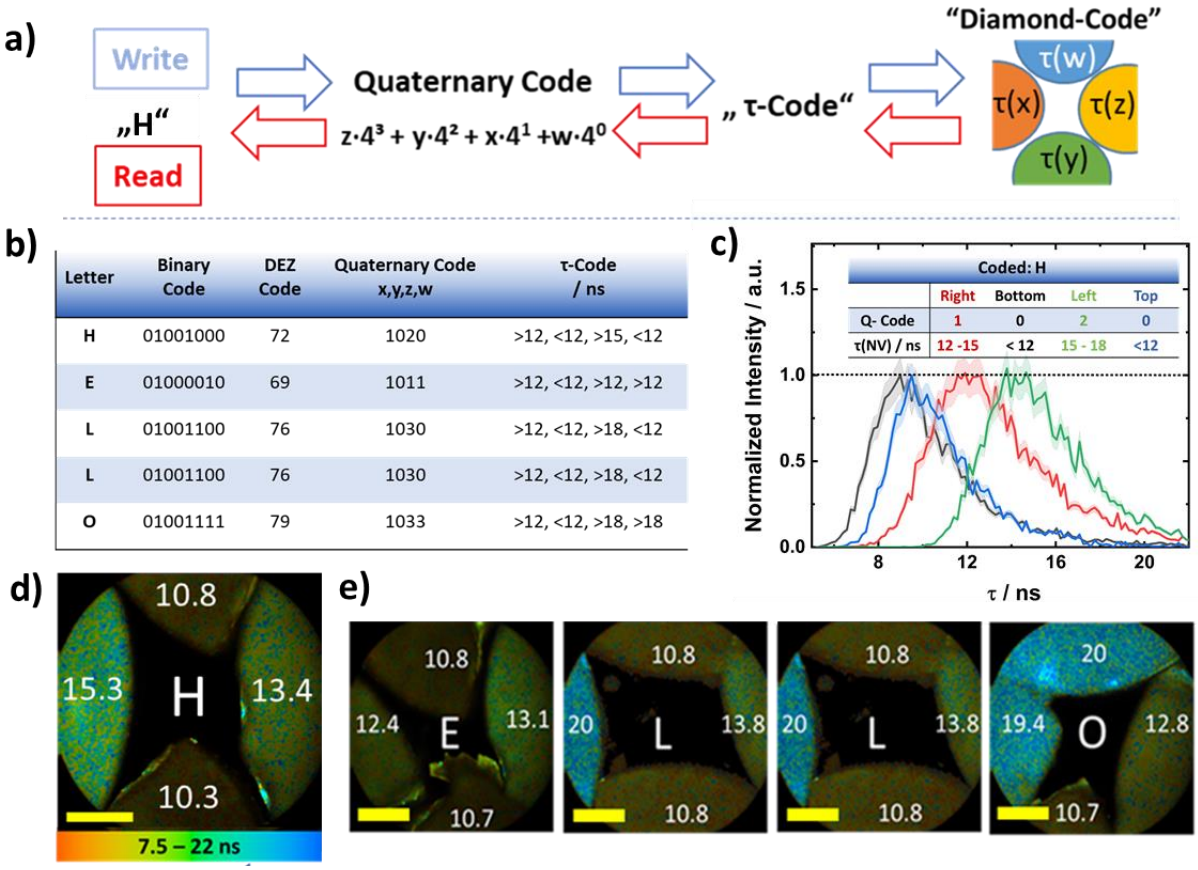

Letter	Binary Code	DEZ Code	Quaternary Code x,y,z,w	τ-Code / ns
H	01001000	72	1020	>12, <12, >15, <12
E	01000010	69	1011	>12, <12, >12, >12
L	01001100	76	1030	>12, <12, >18, <12
L	01001100	76	1030	>12, <12, >18, <12
O	01001111	79	1033	>12, <12, >18, >18

Figure 4 Lifetime coding using NV center in ND: **a)** Schematic illustration of the transcription approach from a DEZ code to Quaternary Code and the final fluorescence lifetime regime code; **b)** Fluorescence lifetime transcription table to write „HELLO“ via a fluorescence lifetime code; **c)** Lifetime histograms of the τ-transcription of the letter „H“, using different fluences of electron irradiation the NV center fluorescence lifetime regimes were tailored and converted to number value of w, x, y, z using equation 1 the number code for ASCII table was calculated and applied; **d)** FLIM a images of the τ-code (time range 7.5 ns to 22 ns) for the letter „H“ via ND pellets consisting of irradiated NDs with different NV center fluorescence lifetimes, scalebar 450 µm; **e)** τ-code for the letters E-0, note L was doubled, scalebar 450 µm.

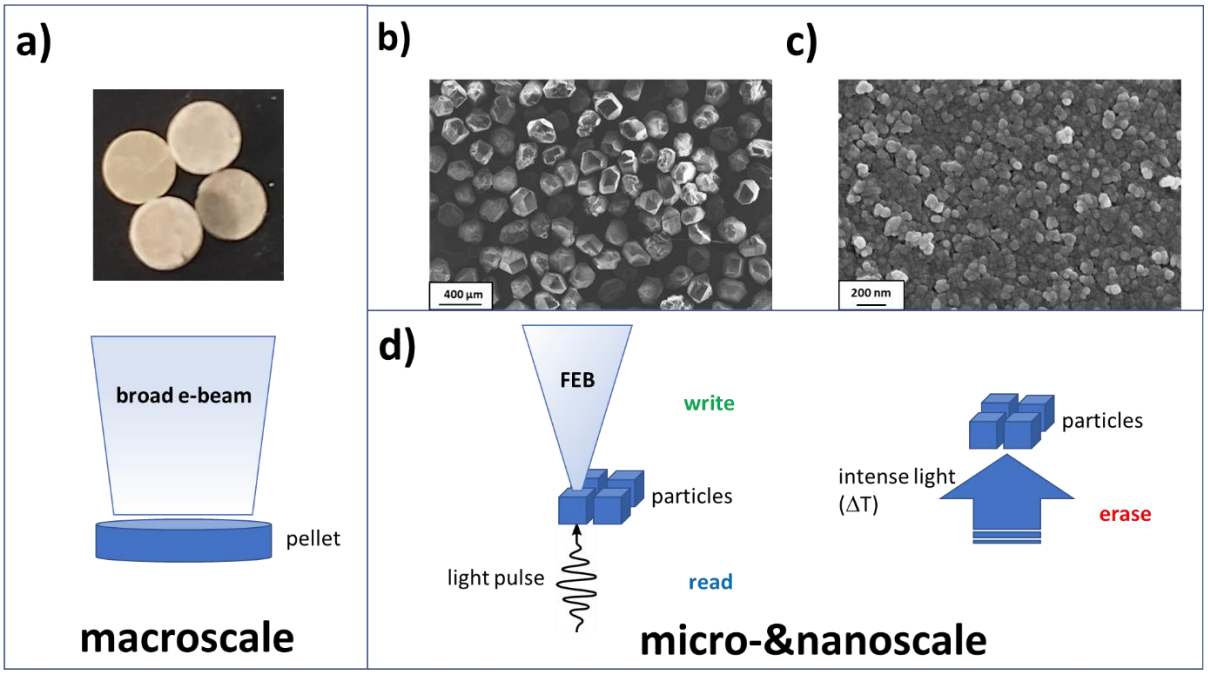

Figure 5 Schematic illustration of the macroscopic **(a)** and a possible micro and nanoscale **(b-d)** experiment using nanodiamonds for data storage: **a)** Macroscopic writing of information via broad electron beam irradiation; **d)** Microscopic writing step, e.g., with a focused electron beam (FEB), the "readout" may be laser-induced optical luminescence detection; the erasing step on the microscopic level can be performed via laser induced optical or global thermal heating.